Expansion of the surrogate method to measure the prompt fission neutron multiplicity for ^{241}Pu

O. A. Akindele,[1,*] B. S. Alan,[2] J. T. Harke,[2] R. J. Casperson,[2] R. O. Hughes,[2] J. D. Koglin,[2] K. Kolos,[2] E. B. Norman,[1] S. Ota,[3] and A. Saastamoinen[3]

[1]*Department of Nuclear Engineering, University of California, Berkeley, California 94720, USA*

[2]*Lawrence Livermore National Laboratory, Livermore, California 94550, USA*

[3]*Cyclotron Institute, Texas A&M University, College Station, Texas 77840, USA*

(Received 2 January 2019; published 1 May 2019)

Fission neutron multiplicity data are imperative for nuclear models that support criticality safety, nuclear nonproliferation, and stockpile stewardship. This work presents the first experimental measurement to determine the average neutron multiplicity ($\bar{\nu}$) and the neutron multiplicity distribution using a surrogate reaction. ^{241}Pu has a short half-life of 14.3 yr. To circumvent experimental difficulties, inelastic scattering of 53.96-MeV α particles on ^{242}Pu served as a surrogate for ^{241}Pu(n, f). The present text reports and discusses the average neutron multiplicity, in addition to the neutron multiplicity moments and distribution for equivalent neutron energies up to 20 MeV. The $\bar{\nu}$ measured in this experiment agrees with previous measurements until 12 MeV, where discrepancies arise due to preequilibrium neutron emission.

DOI: 10.1103/PhysRevC.99.054601

I. INTRODUCTION

Nondestructive assay of fissile material is commonly used to verify the isotopic composition of nuclear material for treaty verification purposes. In these cases, samples of declared material are placed in well counters, and the concentration of specific actinides can be determined using the measured neutron count rate. To reduce uncertainties in the determined fissile concentration, precise nuclear data on the spontaneous fission rate, neutron production cross sections [e.g., (α, n) on oxygen, fluorine, etc.], and the fast-neutron-induced neutron multiplicity for fissile or fissionable material must be known [1,2].

Of the four "major" actinides found in nuclear reactors (^{235}U, ^{238}U, ^{239}Pu, and ^{241}Pu), the nuclear data for prompt fission neutron multiplicities on ^{241}Pu are sparse. Due to its relatively short half-life, 14.3 yr, target manufacturing for these experiments was difficult and required the use of thick impure targets. ^{241}Pu targets with 97% purity were used in both Conde *et al.* and Frehaut *et al.*'s experiments with samples of 20 and 100 mg, respectively, introducing concerns of self-multiplication [3,4]. Additionally, all previous measurements of fission neutron multiplicities were determined using direct reactions and large liquid scintillators, causing large beam-induced neutron backgrounds.

To circumvent the use of thick, unstable targets and beam-related neutron backgrounds, a surrogate reaction utilizing an incident beam of 53.96-MeV α particles inelastically scattering off a ^{242}Pu target was used in the presented work [5]. Through the use of this method, the reaction

$$^{241}\mathrm{Pu} + n \rightarrow {}^{242}\mathrm{Pu}^{*} \rightarrow F_L + F_H + xn \qquad (1)$$

can be replaced with

$$^{242}\mathrm{Pu} + \alpha \rightarrow {}^{242}\mathrm{Pu}^{*} + \alpha' \rightarrow F_L + F_H + xn + \alpha'. \qquad (2)$$

Here $F_L + F_H$ refers to the light and heavy fission fragments, and x is the number of emitted neutrons, n. This method has been previously used to measure both fission cross sections and fission-fragment distributions for isotopes near the same mass region; however this is the first time the surrogate method has been expanded to fission neutron multiplicities [6–11].

II. EQUIVALENT COMPOUND NUCLEUS

The use of a surrogate reaction relies on the Bohr hypothesis, which assumes the decay of a compound nucleus is independent of its formation [12]:

$$\sigma_{n,f}(E_n) = \sum_{J,\pi} \sigma_n^{\mathrm{CN}}(E_{\mathrm{ex}}, \pi, J) G_f(E_{\mathrm{ex}}, \pi, J). \qquad (3)$$

Here the cross section for fission, $\sigma_{n,f}$, is expressed as a product of the probability of forming a compound nucleus, σ_n^{CN}, and the branching ratio of its decay, G_f. The cross sections and branching ratios depend on energy, E; parity, π; and angular momentum, J. At higher excitation energies, one can employ the Weiskopf-Ewing limit, which assumes that the dependencies on angular momentum and parity are negligible [13]:

$$\sigma_{n,f}(E_n) = \sigma_n^{\mathrm{CN}}(E_{\mathrm{ex}}) G_f(E_{\mathrm{ex}}). \qquad (4)$$

To remove systematic uncertainties associated with an absolute measurement, a surrogate ratio is introduced. Here, the reference reaction ^{241}Pu(n, f) is compared to the reference

*Corresponding author: akindele1@llnl.gov; current address: Lawrence Livermore National Laboratory, Livermore, California 94550, USA.

TABLE I. Isotopic concentration of the ^{242}Pu sample used to electroplate the target in this work. Small concentrations of ^{238,239,240,241}Pu and ^{241}Am are present.

Isotope	^{238}Pu	^{239}Pu	^{240}Pu	^{241}Pu	^{242}Pu	^{241}Am
Activity (μCi)	0.29	0.0018	0.028	3.44	2.25	0.25
Mass (μg)	0.017	0.029	0.123	0.033	570.783	0.073
Fraction (%)	0.003	0.005	0.021	0.006	99.952	0.013

reaction ^{242}Pu$(\alpha, \alpha' f)$ with the assumption that

$$\frac{\sigma_{n,f}(E_n)}{\sigma_n^{\mathrm{CN}}(E_{\mathrm{ex}})} = \frac{\sigma_{\alpha,\alpha' f}(E_n)}{\sigma_\alpha^{\mathrm{CN}}(E_{\mathrm{ex}})} \tag{5}$$

is the same [8,14]. Utilizing the surrogate ratio, Eq. (4) is expressed as

$$\sigma_{\alpha,\alpha' f}(E_\alpha) = \sigma_\alpha'^{\mathrm{CN}}(E_\alpha) G_f(E_{\mathrm{ex}}). \tag{6}$$

In the equation above, the cross section for the surrogate reaction, $\sigma_{\alpha,\alpha' f}$, becomes the product of the probability of forming the same compound nucleus with inelastic α scattering instead of neutron capture and the branching ratio of the compound nucleus through fission. Implementing the Bohr hypothesis, the branching ratios in Eqs. (4) and (6) are the same. In the present work, the branching ratio for fission with the emission of neutrons is of interest; thus, the formation of the same excited compound nucleus is used as a tag to measure the branching ratio.

III. EXPERIMENTAL SETUP

The measurement was performed at the Texas A&M University Cyclotron Institute using 53.96-MeV α particles incident on a 140 μg/cm^2 target. The target was made by electroplating ^{242}Pu onto a 100 μg/cm^2 natural carbon backing. Table I shows the isotopic composition of the sample used to make the ^{242}Pu target. The NeutronSTARS array was used to detect and correlate charged particle events and neutron emission [15]. An illustration of the experimental setup can be seen in Fig. 1.

The scattered α particles were detected using a thin ΔE and a thick E silicon detector located downstream of the target. In addition to determining the energy of the charged particles, the silicon telescope was used for particle identification to ensure that tagged events were from scattered α particles and other reaction products. Another silicon detector was also placed upstream of the target to identify fission events by tagging on emitted fragments. A large cylindrical tank segmented into four quadrants and filled with 2.2 tons of EJ-335 was used to detect emitted neutrons. The neutron detection efficiency determined using ^{252}Cf was determined to be $50.81 \pm 0.15\%$. An additional 1% uncertainty is included in the systematic errors to account for the neutron energy dependence for the detection efficiency.

IV. ANALYSIS

In this work, an event is triggered by an α event in the ΔE and E detectors in coincidence with the detection of a fission fragment in the fission detector. Neutrons emitted following this trigger are then measured in the liquid scintillator. During the experiment, multiple events that are not of interest also deposit energy in the ΔE and E silicon detectors, the fission detector, and/or the liquid scintillator. To reduce the contribution of background events from light ions ($m \leqslant 4$ a.m.u.), fusion-fission events, muogenic and spallation events, and other sources of radiation from the room or beam, appropriate cuts to signals identified in multiple detectors must be made.

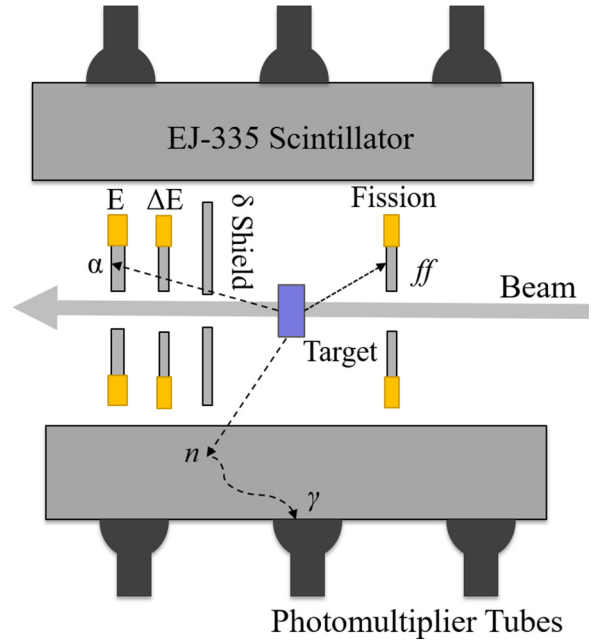

FIG. 1. Cross-sectional view of the detectors used in the experiment relative to the beam line. A silicon telescope is located downstream of the beam for event tagging and particle identification. A silicon detector is located upstream of the target to identify fission events. The entire target chamber is surrounded by a large cylindrical tank filled with EJ-335 and segmented into quadrants, where each quadrant has three photomultiplier tubes mounted on the side.

A. Event selection

To ensure events that trigger the system are from scattered α particles, the energy loss in the ΔE can be plotted against the total energy deposited in the telescope. This was used to identify particles from their unique dE/dx in silicon. The particle identification (PID) equation was used to show a clear separation of particles given their mass and charge [16]:

$$R = 15.0[(E + \Delta E)^{1.75} - E^{1.75}]. \tag{7}$$

Here the exponents are constants that represent the energy loss in silicon for α particles. The resulting PID plot can be seen in Fig. 2. The nuclear structure from ^{242}Pu, oxygen, and carbon are evident in the scattered α-particle band. Making a cut at an effective thickness of 17 500 removes events correlated with ^{3}He, tritons, deuterons, and protons, including "punch through" corresponding to events where ions do not stop in the E detector.

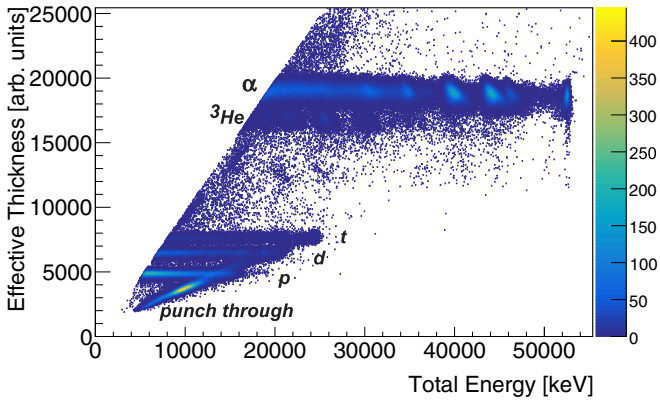

FIG. 2. Linearized particle identification plot as described in the text. Clear separations between α's, ^{3}He, tritium, deuterons, and protons can be seen.

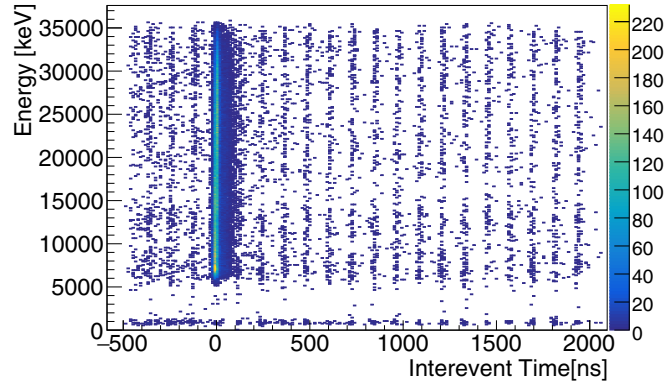

FIG. 3. Fission events coincident with α particles exciting ^{242}Pu and the time difference between the silicon telescope and the fission detector. Correlated events are shown at $t = 0$, while random coincident backgrounds (e.g., elastic scattering in coincidence with fusion-fission) are observed to be correlated with beam pulses associated with the cyclotron's radio frequency.

Following the detection of α particles in the silicon telescope, a coincident fission fragment in the fission detector defines the beginning of an event. Due to the high rate of elastic scattering and fusion-fission, the two occurring in coincidence causes accidental backgrounds. Figure 3 shows the timing correlation between the silicon telescope and the fission detector as a function of excitation energy. To remove the accidental contribution a prompt timing gate is set at -50 to 150 ns, while the background is characterized from 250 to 2000 ns.

The target used in this experiment is a plutonium-oxide electroplated onto a carbon backing. Reactions on oxygen and carbon in the target can induce carbon and oxygen breakup which registers signals in the fission detector. To account for this background, a natural carbon and Mylar ($C_{10}H_8O_4$) target were placed in the beam for 24 and 12 h, respectively. From these two targets the energy deposition in the fission detector from oxygen and carbon contributions, as shown in Fig. 4, did not surpass 40 MeV. Instead of subtracting the contributions of oxygen and carbon, an energy threshold of 40 MeV was set.

When observing the number of fission events as a function of both the excitation energy for ^{242}Pu and the equivalent neutron energy for ^{241}Pu, distinct features relating to nuclear structure, specifically the neutron separation energy, can be observed. As shown in Fig. 5 the fission events at low excitation energy, <5 MeV, are due to accidental coincidence events from elastic scattering off ^{242}Pu, oxygen, or carbon with fusion-fission. The fission rate begins to increase at the neutron separation energy, $S_n = 6.31$ MeV. Features from multichance fission are evident at the other neutron separation energies: 11.6, 18.1, and 23.8 MeV. Beyond an excitation energy of 30.6 MeV the number of measured outgoing α particles falls off due to the Coulomb barrier for α particles incident on ^{242}Pu. Given the lack of statistics past the Coulomb barrier, the measurement is not presented past this energy range.

B. Equivalent neutron energy

The energy of the detected α particle can be reconstructed to determine the equivalent neutron energy. An α-particle beam with energy $E_{\text{beam}} = 53.96$ MeV inelastically scatters on ^{242}Pu. Due to momentum and energy conservation some energy transfer will be lost from the recoil of the nucleus, while the rest will excite the nucleus to another state. In addition to losing some energy in the ΔE before stopping in the E detector, the scattered α particle will also lose energy in various dead layers, i.e., materials that are not active detectors. ELAST, Energy Loss and Straggling Tool, was used to model the energy loss in the δ shield, the gold and aluminum layers surrounding the silicon telescope, and the ^{242}Pu target [17]. The reconstructed excitation energy of ^{242}Pu, E_{ex}, can be represented as follows:

$$E_{\text{ex}} = E_{\text{beam}} - (E_{\text{rec}} + E_{\text{loss}} + \Delta E + E). \tag{8}$$

Here E_{rec} is the energy of the recoiling nucleus and E_{loss} is the energy loss of the α particle through the dead layers. The equivalent neutron energy, E_n, can be determined using the following:

$$E_n = E_{\text{ex}} - S_n. \tag{9}$$

Here S_n is the neutron separation energy for ^{242}Pu. In a neutron-induced reaction when $^{241}\text{Pu} + n$ forms $^{242}\text{Pu}^*$, the resulting compound nucleus is left in an excited state determined by the Q value of the reaction which is equivalent to $-S_n$ for ^{242}Pu and the energy of the incident neutron.

C. Neutron detection

Two timing gates were used to determine the fission neutron multiplicity: a background gate from -42 to -2 μsec and a prompt gate at 2–42 μsec. Energy deposition that exceeded 2 MeV in the liquid scintillator was considered a neutron capture, while events surpassing 12 MeV were neglected to remove contributions from muons and fast-neutron backgrounds. Figure 6 shows the time correlation of events in the scintillator relative to event tags in the silicon telescope and the fission detector. Before a fission event occurs, the energy distribution is relatively flat. At $t = 0$, γ rays from fission and proton recoils are present in the detector. Following

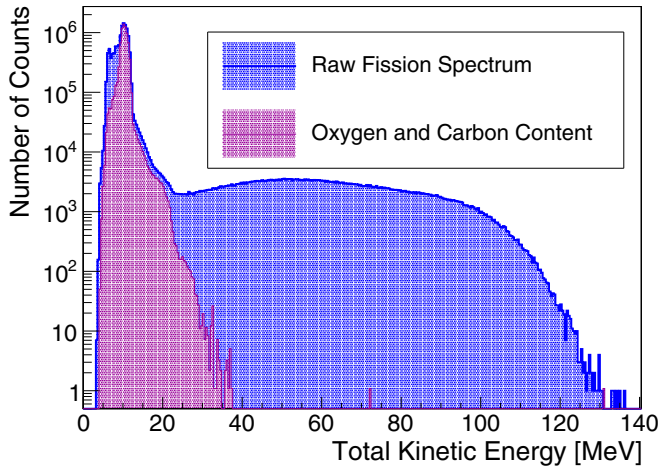

FIG. 4. Energy deposition in the fission detector summed over all excitation energies for ^{242}Pu and the contribution from oxygen and carbon, which was extracted using the measurement of the carbon and Mylar targets. The lower-energy feature is due to the α decay of the target. Above 40 MeV, only contributions from fission fragments can be observed in the detector. The "smearing" of the light and heavy fragments' total kinetic energy is due to the wide angular coverage of the fission detector.

fission, clear separation between the γ flash and the neutron thermalization can be seen.

The flat nature of the background rate would imply a Poisson distribution. However, when observing the neutron multiplicity distribution in the background gate, deviations from this shape occur due to backgrounds correlated from the beam and the target such as fusion-fission and other induced neutron processes. The average neutron multiplicity, $\bar{\nu}$, was determined using events in the prompt gate, p, events in the background gate, b, and the total number of fission triggers,

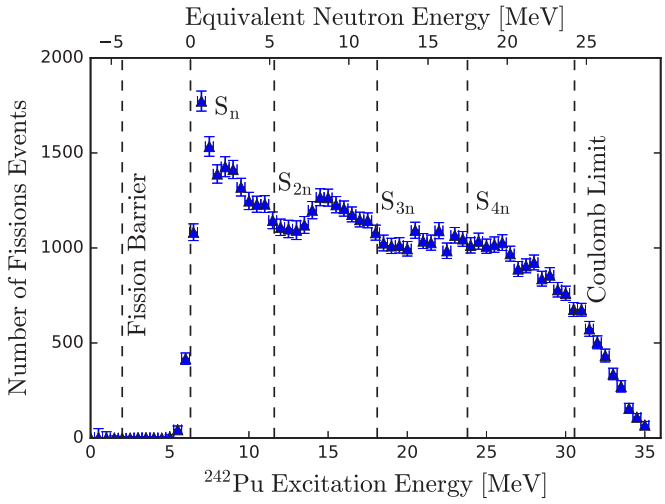

FIG. 5. Fission events as a function of the excitation energy for ^{242}Pu and the equivalent neutron energy for ^{241}Pu. The fission barrier, neutron separation energies, and Coulomb limit are referenced for the excitation energy of the ^{242}Pu nucleus.

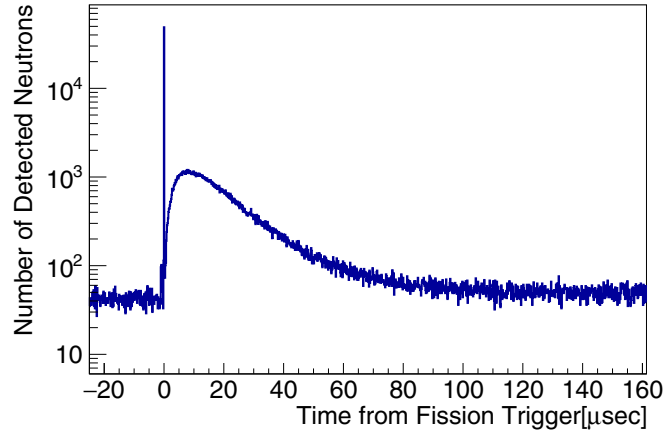

FIG. 6. Time correlation of events in the scintillator relative to the fission event trigger. At negative times the background is flat. The prompt fission γ rays are evident at $t = 0$, while the capture of neutrons is seen on the order of tens of microseconds after fission.

f, as a function of energy, E:

$$\bar{\nu}[E] = \frac{(p[E] - b[E])}{f[E]\varepsilon}. \tag{10}$$

Here ε is the efficiency of the neutron detector.

To determine the neutron multiplicity as a function of energy, the background is subtracted using the following deconvolution:

$$D[i] = P[i, j]^{-1} D'[i]. \tag{11}$$

Here D' is a one-dimensional vector and i corresponds to the detected multiplicity for each integer neutron without background correction. The matrix $P[i, j]$ is an upper diagonal matrix composed of the background multiplicity $b[i]$ for n neutrons:

$$P[i, j] = \begin{cases} b[j - i] & \text{if } j \geqslant i, \\ 0, & \text{otherwise.} \end{cases} \tag{12}$$

The neutron detection efficiency follows a binomial distribution. The matrix expressing the probability that i neutrons were detected for a real multiplicity of j for a given efficiency ϵ is as follows:

$$B[i, j] = \begin{bmatrix} j \\ i \end{bmatrix} \epsilon^i (1 - \epsilon)^{j-i}. \tag{13}$$

To extract the moments associated with the fission neutron multiplicity distribution as a function of E_n, a true multiplicity distribution shape that is convolved with the Neutron ball detector efficiency is assumed. This function is used to fit the present data to deduce the moments. A Gaussian shape has previously been suggested for the neutron multiplicity distribution [1]. In the present work, a skewed Gaussian, G, of the form

$$G[\nu] = \frac{1}{\sqrt{2\pi}\sigma} \exp\left(\frac{(\nu - \mu)^2}{2\sigma^2}\right)\left[1 + \text{erf}\left(\frac{\beta(\nu - \mu)}{\sqrt{2}\sigma}\right)\right], \tag{14}$$

provides superior agreement between the extracted first moment and the directly measured $\bar{\nu}$ in this work (8), so this function is adopted. This approach was also applied to the

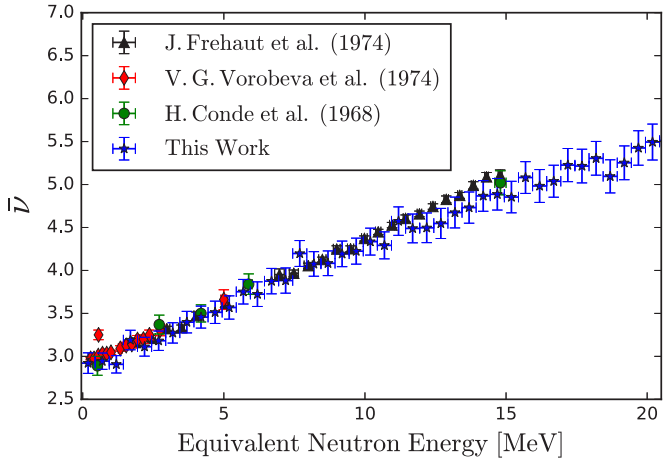

FIG. 7. Results of the average neutron multiplicity for ^{241}Pu compared to the existing literature. The results presented from this work are in agreement with previous measurements and expand the known quantities of $\bar{\nu}$ for ^{241}Pu from 14 MeV up to 23 MeV.

same system with a ^{252}Cf source [15]. The results of the multiplicity were in agreement with literature values.

Traditionally, nuclear models sample a normal distribution to determine the fission neutron multiplicity distribution; however, this method does not account for the high neutron multiplicity tail that is present from fission [1]. To validate this assumption the multiplicity distribution was fit with both a Gaussian distribution, and a skewed Gaussian distribution. It was determined that the fission neutron multiplicity data was in better agreement with the skewed Gaussian distribution when validating the first neutron moment as described in Sec. V.

The fission neutron moments, ν_1, ν_2, and ν_3, as a function of energy can then be determined from the skewed Gaussian distribution:

$$\nu_1 = \sum_{\nu=1}^{\max} \nu P(\nu), \tag{15}$$

$$\nu_2 = \sum_{\nu=2}^{\max} \nu(\nu-1) P(\nu), \tag{16}$$

$$\nu_3 = \sum_{\nu=3}^{\max} \nu(\nu-1)(\nu-2) P(\nu). \tag{17}$$

Here $P(\nu)$ represents the probability of a given neutron multiplicity. Note the first moment is effectively the same as $\bar{\nu}$.

V. RESULTS

The average neutron multiplicity as a function of equivalent neutron energy is displayed in Fig. 7. When compared to the existing literature values, the measurement is in agreement within the uncertainties at all reported energies. A systematic disagreement at 12 MeV is apparent between this work and Frehaut *et al.*'s data [4]. Sources of the disagreement may arise from multiple factors. In Frehaut *et al.*'s experiment the target consisted of 97% ^{241}Pu. Although the isotopic contribution of

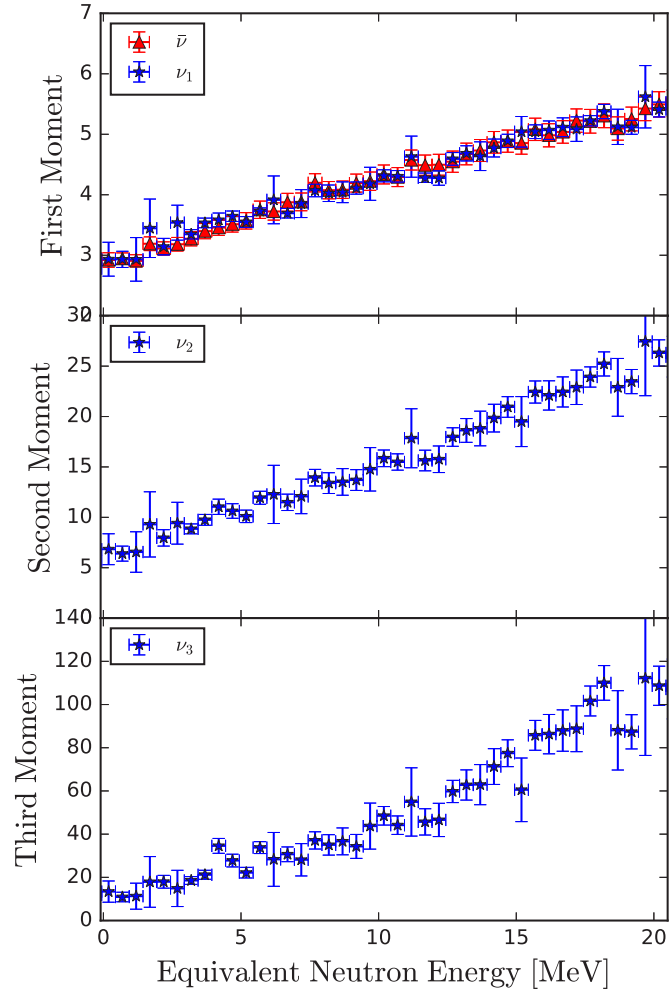

FIG. 8. Derived neutron multiplicity moments for ^{241}Pu as a function of equivalent neutron energy. The first neutron multiplicity moment was compared to the average neutron multiplicity from Fig. 7 as a benchmark to the methodology.

the contaminants are not identified, the purity of the sample is enough to account for the 1% discrepancy. Moreover the target thickness, 20 and 100 mg in the measurements of Conde *et al.* [3] and Frehaut *et al.* [4], respectively, may introduce self-multiplication and multiple interactions in the sample. Pre-equilibrium neutron emission may precede fission in ^{241}Pu(n, f), which will change the excitation energy in the fissioning system. Calculations in TALYS have shown that preequilibrium neutron emission from $(\alpha, \alpha f)$ is expected to be negligible for 53.96-MeV α particles.

Lastly, the 12-MeV energy threshold for the discrepancy is consistent with that of preequilibrium. In a direct reaction a neutron incident on ^{241}Pu may interact with individual nucleons causing an $(n, 2n)$ reaction. If excess energy is left in the residual nucleus it may deexcite through fission. Using (α, α') reactions removes all contributions from preequilibrium for the energy range in this analysis.

After the prompt fission neutron distribution was corrected for background neutrons, the resulting distribution was fit to a skewed Gaussian convolved through the detector response. As a test of the assumed shape to deduce the moments, the first

neutron multiplicity moment was compared to the average neutron multiplicity, which was determined directly. The first neutron moment is effectively the same as the average neutron multiplicity. In Fig. 8, the first neutron moment was consistent with the average neutron multiplicity. By applying Eqs. (16) and (17), subsequent moments were determined, although there are no existing data to compare the results with. The first neutron moment and the average neutron multiplicity moment serves as a benchmark to this approach. The uncertainty increases significantly with the higher-order moments, but similarly to $\bar{\nu}$ the first two moments have linear trends with respect to the equivalent neutron energy.

The deduced P(ν) is consistent with the measured $\bar{\nu}$; further validating the multiplicity distribution at energies where the fit is in reasonable agreement. When observing the neutron multiplicity with increasing incident neutron energy, the spread and the mean increase rather continuously until the nucleus reaches a neutron separation energy. Here, large uncertainties in the fitting parameters occur and the deviations in the multiplicity shape become apparent. This is due to both the limitation in the Weiskopf-Ewing approximation at the threshold of new decay channels becoming available and the superposition of the structure of multiple nuclei due to multichance fission.

VI. CONCLUSION

In summary, both $\bar{\nu}$ and the fission neutron multiplicity moments were determined using the surrogate method for the first time. The results of the measured $\bar{\nu}$ for ^{241}Pu were consistent with the existing literature until the threshold for preequilibrium in neutron-induced reactions at 12 MeV. Although the surrogate method cannot reproduce preequilibrium conditions, this method is suitable for the measurement of average neutron multiplicities below the preequilibrium threshold.

This experiment was also the first time that the fission multiplicity distribution and the neutron multiplicity moments as functions of neutron energy were measured for ^{241}Pu. The results of the fission neutron multiplicity moments displayed a breakdown in the Weiskopff-Ewing approximation at neutron separation energies. Regardless, the first neutron multiplicity moment was consistent with the measured $\bar{\nu}$, allowing for the determination of the second and third neutron multiplicity moments.

Lastly, this measurement introduces a new capability for determining nuclear data. Barring preequilibrium and neutron separation energies, this method replicated past direct neutron measurements. The surrogate method has previously been used to deduce the (n, f) and (n, g) cross sections [18,19]. Extending this method to fission neutron multiplicities allows for a range of experiments to be performed on short-lived nuclei of interest in support of nuclear criticality safety, nonproliferation, and advanced reactor designs.

ACKNOWLEDGMENTS

We thank the staff of the Texas A&M Cyclotron Institute for facilitating operations and facilities needed to perform this measurement. This work was performed under the auspices of the U.S. Department of Energy by Lawrence Livermore National Laboratory under Contract No. DE-AC52-07NA27344, and it was supported by the Department of Energy National Nuclear Security Administration under Grant No. DE-NA0000979 and the Department of Energy National Nuclear Security Administration through the Nuclear Science and Security Consortium under Grants No. DE-NA-0003180. This document was released through information management under No. LLNL-JRNL-736489.

[1] J. P. Lestone, Energy and isotope dependence of neutron multiplicity distributions-LA-U R-05-0288, Los Alamos National Laboratory, Los Alamos, Technical Report (2005).

[2] T. H. Shin, M. Y. Hua, M. J. Marcath, D. L. Chichester, I. Pázsit, A. Di Fulvio, S. D. Clarke, and S. A. Pozzi, Nucl. Sci. Eng. **188**, 246 (2017).

[3] H. Conde, J. Hansen, and M. Holmberg, J. Nucl. Energy **22**, 53 (1968).

[4] J. Frehaut, G. Mosinski, R. Bois, and M. Soleilhac, Measurement of the average number of prompt neutrons emitted in the fission of 240 Pu and 241 Pu induced by neutrons in the energy range 1.5 to 15 MeV, CEA Centre d'Etudes de Bruyeres-le-Chatel, Rapport CEA-R-4626, 1974.

[5] O. Akindele, Expansion of the surrogate method to measure (n, xn) cross sections and fission neutron multiplicity distributions, Ph.D. thesis, University of California, Berkeley, 2018.

[6] J. Koglin, Measurement of plutonium-240 angular momentum dependent fission probabilities using the alpha-alpha' reactions, Ph.D. thesis, The Pennsylvania State University, 2017.

[7] A. Czeszumska, C. T. Angell, J. T. Harke, N. D. Scielzo, E. B. Norman, R. A. E. Austin, G. Boutoux, R. J. Casperson, P. Chodash, R. O. Hughes, C. M. Mattoon, V. Méot, J. Munson, L. Phair, J. J. Ressler, O. Roig, T. J. Ross, E. Swanberg, and B. Wang, Phys. Rev. C **87**, 034613 (2013).

[8] J. T. Harke, L. A. Bernstein, J. Escher, L. Ahle, J. A. Church, F. S. Dietrich, K. J. Moody, E. B. Norman, L. Phair, P. Fallon, R. M. Clark, M. A. Deleplanque, M. Descovich, M. Cromaz, I. Y. Lee, A. O. Macchiavelli, M. A. McMahan, L. G. Moretto, E. Rodriguez-Vieitez, F. S. Stephens, H. Ai, C. Plettner, C. Beausang, and B. Crider, Phys. Rev. C **73**, 054604 (2006).

[9] B. F. Lyles, L. A. Bernstein, J. T. Harke, F. S. Dietrich, J. Escher, I. Thompson, D. L. Bleuel, R. M. Clark, P. Fallon, J. Gibelin, A. O. Macchiavelli, M. A. McMahan, L. Phair, E. Rodriguez-Vieitez, M. Wiedeking, C. W. Beausang, S. R. Lesher, B. Darakchieva, and M. Evtimova, Phys. Rev. C **76**, 014606 (2007).

[10] R. O. Hughes, C. W. Beausang, T. J. Ross, J. T. Harke, N. D. Scielzo, M. S. Basunia, C. M. Campbell, R. J. Casperson, H. L. Crawford, J. E. Escher, J. Munson, L. W. Phair, and J. J. Ressler, Phys. Rev. C **85**, 024613 (2012).

[11] R. J. Casperson, J. T. Harke, N. D. Scielzo, J. E. Escher, E. McCleskey, M. McCleskey, A. Saastamoinen, A. Spiridon, A. Ratkiewicz, A. Blanc, M. Kurokawa, and R. G. Pizzone, Phys. Rev. C **90**, 034601 (2014).

[12] N. Bohr, Nature (London) **137**, 344 (1936).

[13] J. E. Escher and F. S. Dietrich, Phys. Rev. C **81**, 024612 (2010).
[14] C. Plettner *et al.*, Phys. Rev. C **71**, 051602(R) (2005).
[15] O. Akindele, R. Casperson, B. Wang, J. Harke, R. Hughes, S. Fisher, A. Saastamoinen, and E. Norman, Nucl. Instrum. Methods Phys. Res., Sect. A **872**, 112 (2017).
[16] F. S. Goulding and D. A. Landis, Recent advances in particle identifiers at berkeley, in *Semiconductor Nuclear-Particle Detectors and Circuits* (National Academy of Sciences, Washington, DC, 1969), p. 757.
[17] Energy Loss and Straggling Tool, Adapted from the computer program ENELOSS written by H. Ernst (1981) modified by stopping power routines by K. Lesko (1984).
[18] J. J. Ressler *et al.*, Phys. Rev. C **83**, 054610 (2011).
[19] J. M. Munson, E. B. Norman, J. T. Harke, R. J. Casperson, L. W. Phair, E. McCleskey, M. McCleskey, D. Lee, R. O. Hughes, S. Ota, A. Czeszumska, P. A. Chodash, A. J. Saastamoinen, R. A. E. Austin, A. E. Spiridon, M. Dag, R. Chyzh, M. S. Basunia, J. J. Ressler, and T. J. Ross, Phys. Rev. C **95**, 015805 (2017).